Solar Phys (2008) 252: 349–372
DOI 10.1007/s11207-008-9255-z

The Recovery of CME-Related Dimmings and the ICME's Enduring Magnetic Connection to the Sun

G.D.R. Attrill · L. van Driel-Gesztelyi · P. Démoulin · A.N. Zhukov · K. Steed · L.K. Harra · C.H. Mandrini · J. Linker

Received: 21 February 2008 / Accepted: 23 July 2008 / Published online: 13 September 2008

Abstract It is generally accepted that transient coronal holes (TCHs, dimmings) correspond to the magnetic footpoints of CMEs that remain rooted in the Sun as the CME expands out into the interplanetary space. However, the observation that the average intensity of the 12 May 1997 dimmings recover to their pre-eruption intensity in SOHO/EIT data within 48 hours, whilst suprathermal unidirectional electron heat fluxes are observed at 1 AU in the related ICME more than 70 hours after the eruption, leads us to question why and how the dimmings disappear whilst the magnetic connectivity is maintained. We also examine two

Electronic supplementary material The online version of this article (http://dx.doi.org/10.1007/s11207-008-9255-z) contains supplementary material, which is available to authorized users.

G.D.R. Attrill (✉) · L. van Driel-Gesztelyi · K. Steed · L.K. Harra
Mullard Space Science Laboratory, University College London, Holmbury St. Mary, Dorking, Surrey, RH5 6NT, UK
e-mail: gdra@mssl.ucl.ac.uk

L. van Driel-Gesztelyi · P. Démoulin
Observatoire de Paris, LESIA, UMR 8109 (CNRS), 92195 Meudon Principal Cedex, France

L. van Driel-Gesztelyi
Konkoly Observatory of the Hungarian Academy of Sciences, Budapest, Hungary

A.N. Zhukov
Solar-Terrestrial Center of Excellence – SIDC, Royal Observatory of Belgium, Avenue Circulaire 3, 1180 Brussels, Belgium

A.N. Zhukov
Skobeltsyn Institute of Nuclear Physics, Moscow State University, 119992 Moscow, Russia

C.H. Mandrini
Instituto de Astronomía y Física del Espacio, CONICET-UBA, CC. 67, Suc. 28, 1428 Buenos Aires, Argentina

J. Linker
Science Applications International Corporation, 10260 Campus Point Drive, San Diego, CA 92121, USA

other CME-related dimming events: 13 May 2005 and 6 July 2006. We study the morphology of the dimmings and how they recover. We find that, far from exhibiting a uniform intensity, dimmings observed in SOHO/EIT data have a deep central core and a more shallow extended dimming area. The dimmings recover not only by shrinking of their outer boundaries but also by internal brightenings. We quantitatively demonstrate that the model developed by Fisk and Schwadron (*Astrophys. J.* **560**, 425, 2001) of interchange reconnections between "open" magnetic field and small coronal loops is a strong candidate for the mechanism facilitating the recovery of the dimmings. This process disperses the concentration of "open" magnetic field (forming the dimming) out into the surrounding quiet Sun, thus recovering the intensity of the dimmings whilst still maintaining the magnetic connectivity to the Sun.

Keywords Magnetic fields · Corona · Quiet Sun · Coronal mass ejections · Low coronal signatures

1. Introduction

1.1. What are Dimmings?

Transient dimming of coronal intensity, or in short "dimmings", are most often observed as decreases in intensity in soft X-rays (Sterling and Hudson, 1997) and extreme ultra-violet (EUV) data (Thompson *et al.*, 1998), although they were originally observed in ground-based coronagraph data (Hansen *et al.*, 1974). In the first space-based observations with soft X-ray *Skylab* data (Vaiana *et al.*, 1977), dimmings were first referred to as transient coronal holes (TCHs; Rust, 1983), since the intensity of these regions was observed to be similar to that of established coronal holes. More recently, dimmings have been identified in ground-based observations made in the He I 10830 Å line, where they appear as brightenings believed to be induced by a decrease in the overlying coronal radiation (de Toma *et al.*, 2005).

Dimmings have been recognised as being closely associated with coronal mass ejections (CMEs) (Rust and Hildner, 1976), and are now widely acknowledged as a reliable indicator of front-side CMEs (Thompson *et al.*, 2000; Hudson and Cliver, 2001). In classical "double dimming" events (*e.g.* 7 April 1997, 12 May 1997), it was suggested that the dimmings mark the position of the footpoints of an erupted flux rope that makes up the core magnetic field of the associated CME (Sterling and Hudson, 1997; Webb *et al.*, 2000). Upon eruption, the magnetic loops rooted in the dimming regions greatly expand to heights much larger than the gravitational scale height of the plasma. As a result, the plasma can escape the corona and the dimming regions are believed to exhibit a decrease in intensity as the plasma expands or escapes along the "open" field lines (Thompson *et al.*, 2000).

Although plasma evacuation is a widely accepted interpretation of the dimming signature, it should be noted that a decrease in intensity in coronal plasma may be caused by cooling as well as by density depletion (Thompson *et al.*, 1998; Chertok and Grechnev, 2003). However, the observation of dimmings at the same spatial location, in several different wavelengths simultaneously, suggests that such dimmings cannot simply be explained as a temperature effect (*e.g.* Zarro *et al.*, 1999). Indeed, Hudson, Acton, and Freeland (1996) showed that the timescale of the dimming formation observed in *Yohkoh*/Soft X-ray Telescope (SXT; Tsuneta *et al.*, 1991) data is much faster than corresponding conductive and radiative cooling times. More recently, data obtained by the *Hinode*/Extreme ultra-violet

Imaging Spectrometer (EIS; Culhane *et al.*, 2007) have shown a detection of Doppler blue-shifted plasma outflows of velocity ≈ 40 km s^{-1} corresponding to a coronal dimming (Harra *et al.*, 2007b). This result confirms a similar finding (Harra and Sterling, 2001) obtained with the SOHO/Coronal Diagnostic Spectrometer (CDS; Harrison *et al.*, 1995). Imada *et al.* (2007) find that *Hinode*/EIS data of a dimming shows a dependence of the outflow velocity on temperature, with hotter lines showing a stronger plasma outflow (up to almost 150 km s^{-1}). These works collectively support the interpretation of coronal dimmings as being due to plasma evacuation.

1.2. How are Coronal Dimmings Related to Interplanetary Observations?

Assuming that the CME is mostly rooted in the dimmings, several properties derived from the study of dimmings can be used to obtain information about the associated CME: Firstly, calculations of the emission measure and estimates of the volume of dimmings can give a proxy for the amount of plasma making up the CME mass (Sterling and Hudson, 1997; Zhukov and Auchère, 2004). Secondly, the spatial extent of coronal dimmings can give information regarding the angular extent of the associated CME (Thompson *et al.*, 2000; Attrill *et al.*, 2007). Thirdly, quantitative measurement of the magnetic flux through dimmings can be compared to the magnetic flux of modelled magnetic clouds (MC) at 1 AU (Webb *et al.*, 2000; Mandrini *et al.*, 2005; Attrill *et al.*, 2006; Qiu *et al.*, 2007); see Démoulin (2008) for a review. Fourth, studying the evolution of the dimmings, particularly during their recovery phase, can give information about the evolution of the CME post-eruption (Attrill *et al.*, 2006). Finally, study of the distribution of the dimmings, their order of formation and measurement of their magnetic-flux contribution to the associated CME enabled Mandrini *et al.* (2007) to derive an understanding of the CME interaction with its surroundings in the low corona for the case of the complex 28 October 2003 event.

Interplanetary observations can be used to derive physical parameters of the associated interplanetary CME (ICME). If the following characteristics are present: a lower proton temperature and a stronger magnetic field than in the surrounding solar wind, which also exhibits a smooth and significant rotation, then these ICMEs are called magnetic clouds (Burlaga *et al.*, 1981). Solar energetic particles, such as bidirectional electron heat fluxes, can be utilised as diagnostic tracers of the large-scale structure and topology of the interplanetary magnetic field embedded within ICME/MC events (Malandraki *et al.*, 2005). In the context of a closed-field configuration, bidirectional flows are understood to result from particle circulation and reflection; the absence of electron heat fluxes is interpreted as a full disconnection; whilst in an "open" field configuration (where the ICME/MC is connected to the Sun only at one end), the expectation is to observe uni-directional electron heat fluxes (Richardson, Farrugia, and Burlaga, 1991; Shodhan *et al.*, 2000). However, it should be noted that the enhanced magnetic-field regions associated with CME-driven shocks can act to mirror the energetic particles and hence can also produce bidirectional flows (Malandraki *et al.*, 2005). Although this "connectivity indicator" is applied in general, intermittency can be present in the electron-flux distribution with many abrupt, discontinuous dropouts in electron fluxes (see, *e.g.*, Larson *et al.*, 1997; Shodhan *et al.*, 2000). It has been suggested that these dropouts may be due to disconnection of the interplanetary magnetic field from the corona (McComas *et al.*, 1989). Larson *et al.* (1997) noted that the disconnections "presumably result from magnetic reconnection near the Sun". If so, then the heat-flux dropouts might correspond to the regions of "open" field lines in the dimming which have become closed in the corona during the recovery of the dimming. More recently, Crooker and Webb (2006) and Attrill *et al.* (2006) observationally

demonstrated that the negative heat flux in a MC disappeared not because of disconnection, but rather due to a global-scale interchange reconnection (Crooker, Gosling, and Kahler, 2002) between the erupting CME flux rope and the north-polar-coronal-hole magnetic field. Owens and Crooker (2007) have developed a quantitative model of the heliospheric flux and predictions of suprathermal electron signatures which supports the observational conclusions of Attrill *et al.* (2006) and Crooker and Webb (2006). Whilst there are uncertainties associated with using electron heat-flux distributions as indicators of magnetic connectivity (Riley, Gosling, and Crooker, 2004), for the purposes of this work we adopt the interpretation of the general "connectivity indicator" described above.

1.3. Questions Concerning the Relationship Between Dimmings and ICMEs

Despite the often assumed association between dimmings and ICMEs/MCs, Kahler and Hudson (2001) have questioned why coronal dimmings are often observed to disappear well before the associated MCs reach 1 AU. If the identification of coronal dimmings as the footpoints of the expanded erupted magnetic flux rope is correct (as indeed seems plausible given the works of Webb *et al.*, 2000; Mandrini *et al.*, 2005; Attrill *et al.*, 2006), then we need to understand why and how dimmings disappear despite the magnetic connectivity to the Sun being maintained as indicated by electron heat-flux measurements at 1 AU.

In search of answers, in this study we examine the recovery in intensity of dimmings using SOHO/EUV Imaging Telescope (EIT) data and examine the results in the context of interplanetary detection of the associated ICME/MC. We examine three CME-dimming events: 12 May 1997, 13 May 2005, and 6 July 2006, studying the morphology of the dimmings and how they evolve. We discuss the interplanetary *in situ* data for the three events in Section 2, present our analysis and results of the solar data in Section 3, critically discuss the results and suggest a possible physical mechanism for the recovery of the dimmings in Section 4, and conclude in Section 5.

2. The Interplanetary Signatures of the CME-Related Dimming Events

2.1. 12 May 1997 Event

This is a much-studied "classical" dimming event, originating from NOAA AR 8038, and associated with a long-duration C1.3 class flare, a diffuse coronal wave and a halo CME. The evolution and magnetic nature of these unidentical twin dimmings was studied in detail by Attrill *et al.* (2006). The interpretation of this event by Webb *et al.* (2000) that the dimmings marked the footpoints of the associated erupted flux rope is strongly supported by both studies.

Figure 1(a) shows data from the Magnetic Field Investigation (MFI) (Lepping *et al.*, 1995), aboard the *WIND* spacecraft. *In situ* magnetic observations (three-second temporal cadence) were obtained by the MFI instrument. The data were downloaded from the public database http://cdaweb.gsfc.nasa.gov/cdaweb/istppublic/. Figure 1 shows the magnetic-field vector components measured in the Geocentric Solar Ecliptic (GSE) system. The *WIND* 3D Plasma and Energetic Particle experiment (3DP; Lin *et al.*, 1995) electron spectrogram data (displayed in the bottom panels of Figure 1) were downloaded from http://sprg.ssl.berkeley.edu/wind3dp/esahome.html. In the interval identified as the MC (10:00 UT 15 May to 01:00 UT 16 May (Webb *et al.*, 2000; Attrill *et al.*, 2006) – between vertical dashed lines in Figure 1(a)), there is a weak unidirectional electron heat flux (green,

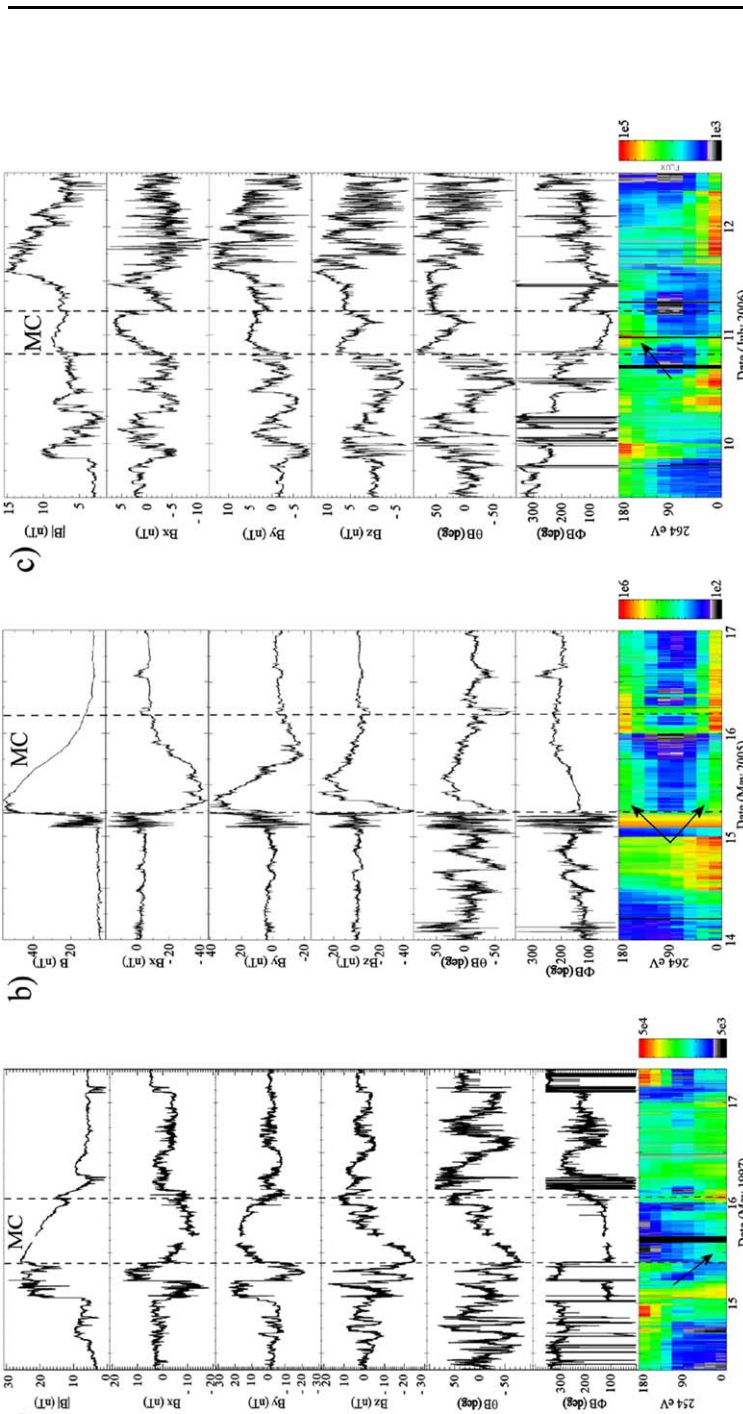

Figure 1 Interplanetary data from the *WIND* and ACE spacecraft showing the relationship between the MC and electron heat fluxes for the three events (a) 12 May 1997, (b) 13 May 2005, and (c) 6 July 2006, respectively. Vertical dashed lines indicate the duration of the magnetic cloud for each event. The first four panels of each plot (reading from top to bottom) show the interplanetary magnetic field (IMF) and its components. The fifth panel shows the θ angle of the IMF vector, with time, where θ is the angle between the ecliptic plane (defined by X_{GSE}, Y_{GSE}) and the IMF in GSE coordinates. The sixth panel shows the ϕ angle of the IMF with time, where ϕ is the angle between X_{GSE} and the projection of the IMF in GSE onto the ecliptic plane. The bottom panels show the pitch-angle distribution of the energetic electron heat fluxes. Black arrows indicate the electron streams within the magnetic clouds.

indicated by the black arrow), starting at 10:00 UT on 15 May. This unidirectional electron stream is directed parallel to the magnetic field (pitch angle 0°) and so is understood to originate from a positive polarity source on the Sun.

2.2. 13 May 2005 Event

This full-halo CME event originating from NOAA AR 10759 was associated with a long-duration M8.0 class flare and a diffuse coronal wave. The event has been studied by Yurchyshyn *et al.* (2006) and Qiu *et al.* (2007), who both examine the solar data and interplanetary counterpart. Liu *et al.* (2007) concentrate their study on the detailed process of the sigmoid eruption. The event is also under study by the SHINE community. In some ways it is perceived to be a similar event to 12 May 1997. However, despite the apparently similar "double dimming" signature, there are key differences. Namely, this event takes place during the declining phase of the last solar cycle, not during the rising phase of a new cycle. As such, the background magnetic field is considerably more complex than that of 12 May 1997. Figure 1(b) (panels 1 – 6) shows data from the Magnetometer instrument (MAG) (Smith *et al.*, 1998), onboard the ACE spacecraft. *In situ* magnetic observations were obtained at a temporal cadence of 16 seconds. The bottom panel of Figure 1(b) shows the *WIND* 3DP electron spectrogram data. Yurchyshyn *et al.* (2006) identify bidirectional heat flux (green, indicated by black arrows) between 05:30 UT 15 May – 08:00 UT 18 May 2005 and place the boundaries of the MC from 06:00 UT – 19:12 UT on 15 May. Qiu *et al.* (2007) identify the start of the MC at 05:40 UT on 15 May, stating its duration as being 23 hours, taking the "end" of the MC to 04:40 UT on 16 May.

2.3. 6 July 2006 Event

This event also exhibits the classical "double dimmings" signature. The halo CME originated from NOAA AR 10898 and was associated with an M2.5 class flare and a diffuse coronal wave. The onset of the event was studied in detail by Jiang *et al.* (2007) and the recovery phase has been examined by McIntosh *et al.* (2007). Figure 1(c) shows data from the ACE/MAG instrument at a temporal cadence of 16 seconds. The bottom panel shows electron-spectrogram data from *WIND* 3DP. A MC is identified between approximately 21:30 UT on 10 July and 06:00 UT 11 July. There are three intervals that show evidence for uni-directional suprathermal electron signatures. The interval closest in time with the MC is between 21:30 UT on 10 July to 04:15 UT on 11 July. In this interval, there are unidirectional electrons (green, indicated by a black arrow) at 180° to the magnetic field, which are understood to originate from a negative-polarity source.

3. Solar Data Analysis and Results

We use SOHO/EIT (Delaboudinière *et al.*, 1995) 195 Å full-disk images, at approximately 17, 17, and 12 minute intervals with pixel sizes of 5.26″, 5.26″, and 2.63″ for the 12 May 1997, 13 May 2005, and 6 July 2006 events, respectively. All EIT heliograms are differentially de-rotated to the same pre-event time at the start of each dataset, using the *SolarSoft* `drot_map` routine. This routine corrects for the latitudinal dependence of the solar differential-rotation function, however we note that projection effects in the derotated 3D corona still remain in the data. The 12 May 1997 dataset runs from 00:12 UT on 12 May 1997 until 23:55 UT on 13 May 1997 before limb brightening/darkening effects, due to the

de-rotation, make a significant contribution to the region where the main dimmings are located. Similarly, the 13 May 2005 dataset runs from 14:05 UT on 13 May until 13:46 UT on 15 May 2005, and the 6 July 2006 dataset runs from 03:54 UT on 6 July until 19:48 UT on 7 July 2006.

To visualise the dimmings clearly, we produce base-difference images where the same pre-event image is subtracted from all subsequent images. We use base-difference images because false dimmings can be created when using the running-difference method (Chertok *et al.*, 2004; Chertok and Grechnev, 2005). In order to carefully analyse the evolution of the dimmings, we need to impose reproducible and quantifiable boundaries. We use the contour method described in Section 2.2 of Attrill *et al.* (2006) where iso-contour brightness levels are set to lie halfway between the intensity of an area of the quiet Sun and that of an existing coronal hole. We choose reference coronal hole and quiet Sun regions that are far from the source region of the CME and are as large in area as is feasible. For the 12 May 1997 event, a region in the south polar coronal hole centred at $(-80'', -860'')$ extending $100''$ in each direction is used and the quiet-Sun reference level is from a region centred at $(-560'', 170'')$, extending $100''$ in each direction. For the 13 May 2005 event, a region in the north-polar coronal hole centred at $(-135'', 890'')$ extending $75''$ in each direction is used and the quiet-Sun reference level is from a region centred at $(-400'', -265'')$, extending $100''$ in each direction. For the 6 July 2006 event, a region in the north-polar coronal hole centred at $(30'', 880'')$ extending $75''$ in each direction is used and the quiet-Sun reference level is from a region centred at $(-390'', -70'')$, extending $100''$ in each direction.

3.1. Contours Showing Contraction of the Dimmings

Figures 2, 3, and 4 show EIT 195 Å heliograms with the dimmings near their maximum spatial extent for the 12 May 1997, 13 May 2005, and 6 July 2006 events, respectively. The top right panels of each figure show a corresponding base difference image, overlaid on which are contours calculated at the times shown during the recovery phase of the dimmings. The shrinking of the contours reflects the shrinking of the spatial extent of the dimmings which occurs in a fragmentary, inhomogeneous, gradual manner; a recovery from the outer boundary inward. Table 1 quantifies the change in area of the dimmings. The evolution of the contour plots (Figures 2, 3, and 4) can also be viewed as movies.

In the 12 May 1997 event (Figure 2) shrinking of the spatial extent of both of the dimmings is clearly visible. The northernmost part of dimming 1 shows a larger contraction than the periphery of dimming 2. We refer the interested reader to Attrill *et al.* (2006) and Crooker and Webb (2006) where this more substantial spatial recovery is attributed to a large-scale interchange reconnection between the magnetic field of the expanding CME rooted in dimming 1 and the "open" magnetic field of the north polar coronal hole.

Identified as a "twin dimmings" event in the literature, the evolution of the 13 May 2005 dimmings (Figure 3) is clearly asymmetric and more complex than that of the 12 May 1997 event. The only region which shows a clear contraction in the time-scale covered by our dataset is the southern part of dimming 2. Liu *et al.* (2007) note that an extension to the South of dimming 2 went on to develop "into an elongated transequatorial coronal-hole".

The 6 July 2006 event exhibits clear contraction of only dimming 2 (Figure 4) in all directions. Although dimming 1 shows a contraction from the Northeast, the extent of the rest of this region remains constant throughout our dataset – a notable feature that also applies to the scattered dimmings surrounding dimming 1.

3.2. Intensity Profiles Showing Internal Brightening of the Dimmings

Overlaid on both the EIT intensity heliogram and base-difference image in Figures 2, 3, and 4 is a red line which passes through the longest-lived part of each dimming. From here on,

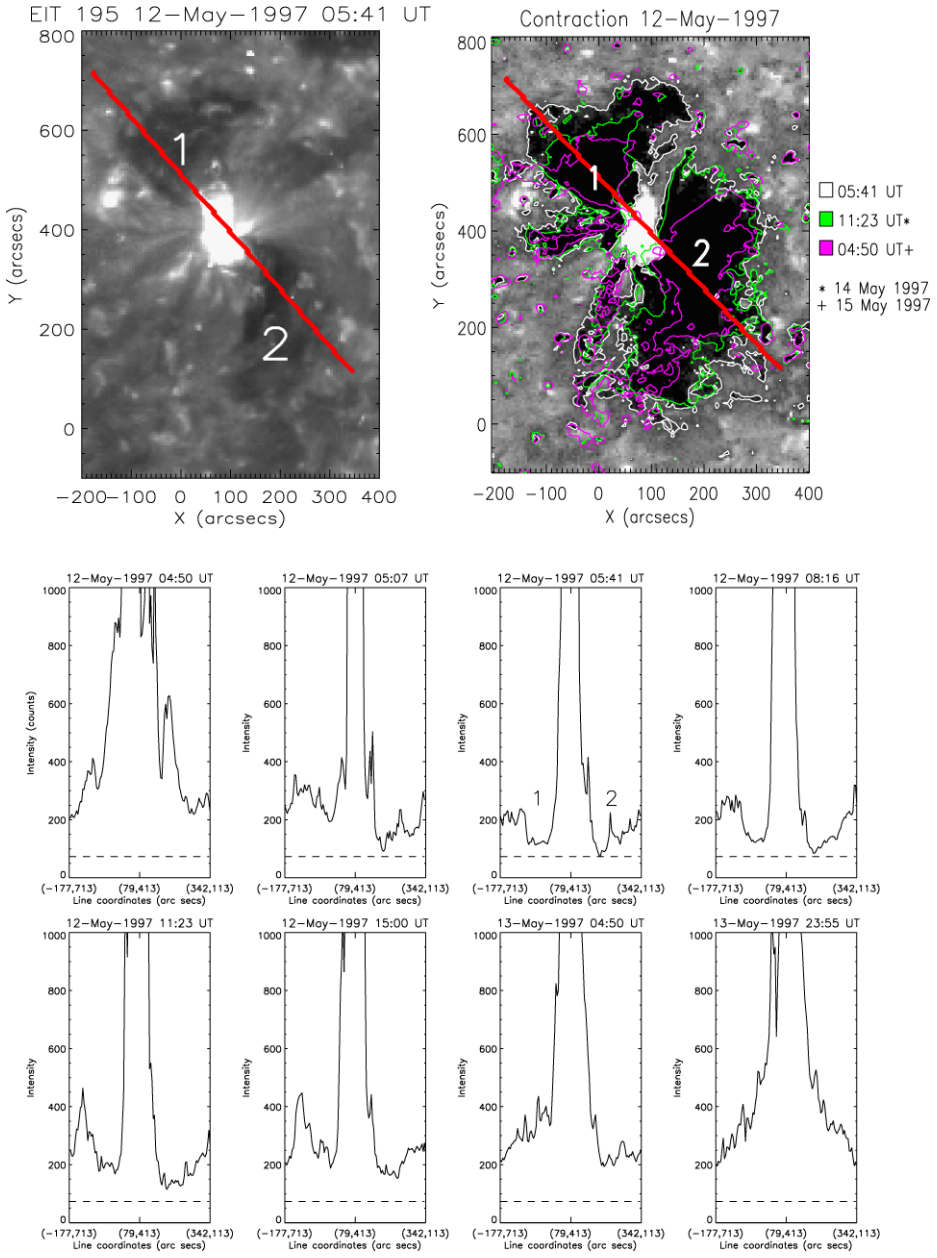

Figure 2 The top left panel is an EIT intensity heliogram showing the 12 May 1997 dimmings. The top right is a base-difference image showing the dimmings, with contours overlaid at the times shown in the colour bar. This plot is best viewed as a movie showing the evolution of these dimmings and is available as electronic supplementary material with the online version of this article (see first page footnote). The red line overlaid on both figures shows the location of the data used to produce the following intensity profile plots. Bottom: Intensity profile plots made along the red line across the cores of the dimmings, at various times during the dimming recovery. The dimmings are identified by the numbers 1 and 2. The dashed line shows the deepest dimming level reached inside the dimmings in this time series.

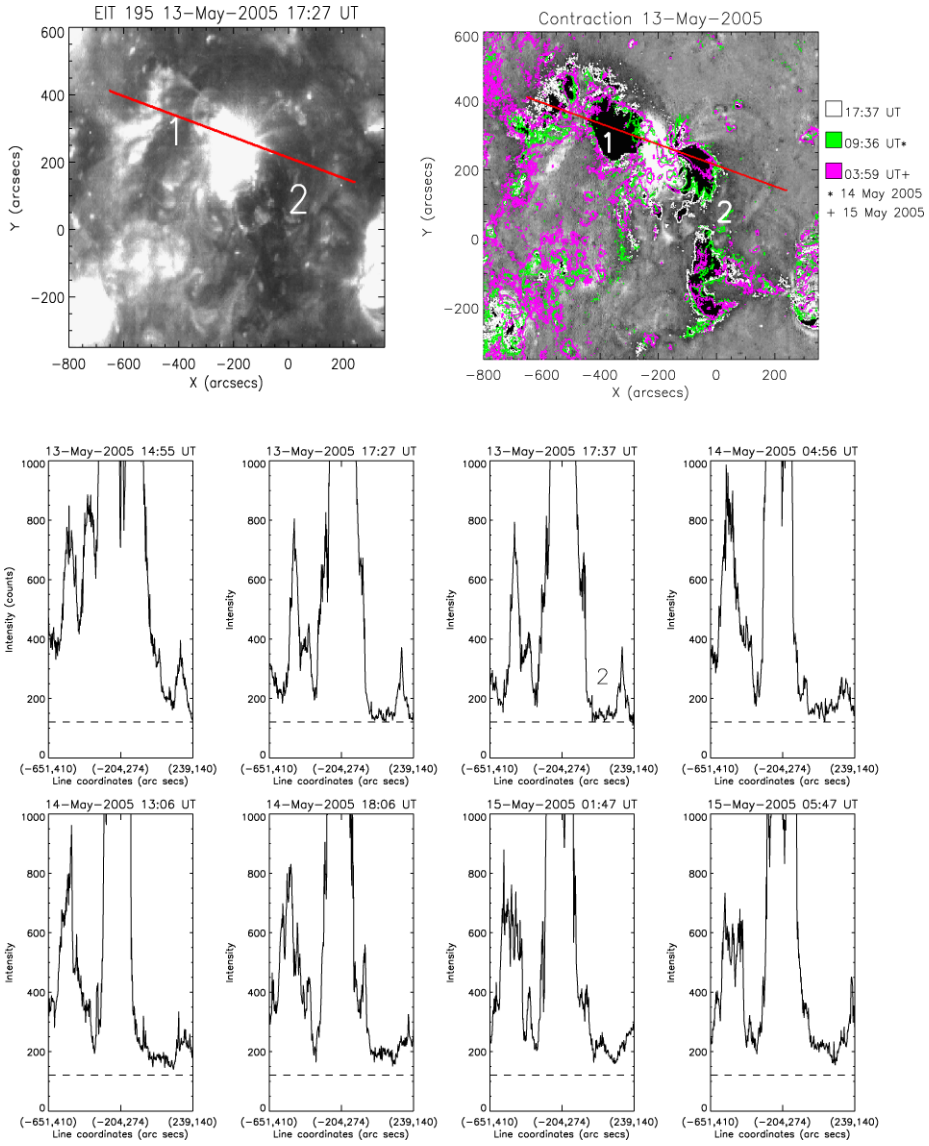

Figure 3 The top left panel is an EIT intensity heliogram showing the 13 May 2005 dimmings. The top right is a base difference image showing the dimmings, with contours overlaid at the times shown in the colour bar. This plot is best viewed as a movie showing the evolution of these dimmings and is available as electronic supplementary material with the online version of this article (see first page footnote). The red line overlaid on both figures shows the location of the data used to produce the following intensity profile plots. Bottom: Intensity profile plots made along the red line across the cores of the dimmings, at various times during the dimming recovery. Dimming 2 is identified by the number 2. The dashed line shows the deepest dimming level reached inside the dimmings in this time series.

we refer to the longest-lived part of the dimming as the "core". Below the heliograms are a time series of intensity profiles (from the EIT intensity heliogram data) made along each red line. The top-left intensity profile shows the intensity along the red line before the event and

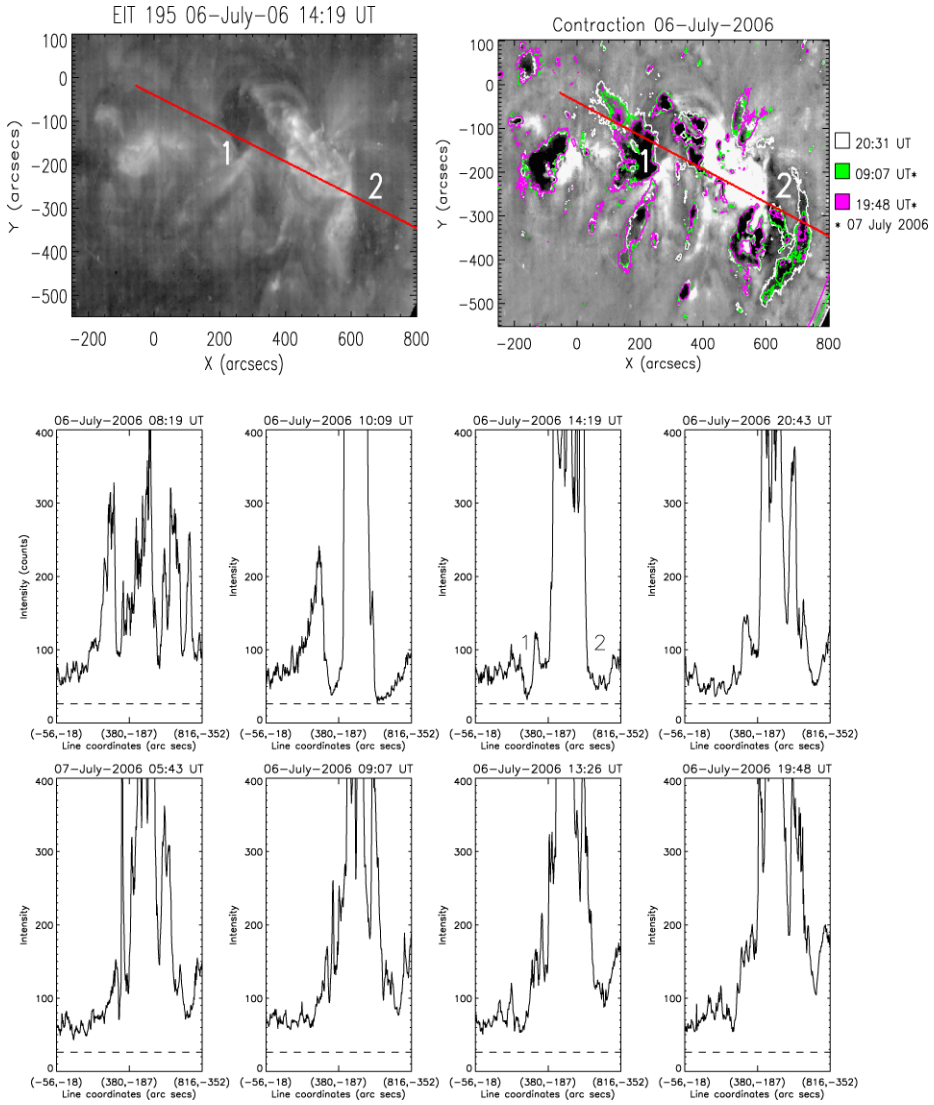

Figure 4 The top left panel is an EIT intensity heliogram showing the 6 July 2006 dimmings. The top right is a base difference image showing the dimmings, with contours overlaid at the times shown in the colour bar. This plot is best viewed as a movie showing the evolution of these dimmings and is available as electronic supplementary material with the online version of this article (see first page footnote). The red line overlaid on both figures shows the location of the data used to produce the following intensity profile plots. Bottom: Intensity profile plots made along the red line across the cores of the dimmings, at various times during the dimming recovery. The dimmings are identified by the numbers 1 and 2. The dashed line shows the deepest dimming level reached inside the dimmings in this time series.

the other profiles show snapshots during the recovery process, following the eruption. The intensity profiles clearly show an increase in intensity within the dimmings for each event.

For the 12 May 1997 event (Figure 2), both dimming regions 1 and 2 can be identified in the intensity profiles. Dimming 2 reaches a lower intensity level than dimming 1. During the time series, both dimmings show a gradual increase in brightness. The 13 May

Table 1 Area and difference (dArea) in units of 10^{10} km^2 of the dimmings defined by the white, yellow, green, and blue contours in the movies accompanying Figures 2, 3, and 4 for each of the three events. dTime is the time difference between contours (in hours). dArea/dTime is the rate of change of the dimming areas (in units of 10^5 km^2 s^{-1}).

Contour & Time	Area	dArea	dTime	$\frac{\text{dArea}}{\text{dTime}}$	Area	dArea	dTime	$\frac{\text{dArea}}{\text{dTime}}$
12 May 1997	dimming 1				dimming 2			
White 05:41 UT	3.50				5.15			
		0.95	2.58	−10.2		0.54	2.58	−5.81
Yellow 08:16 UT	2.55				4.61			
		0.70	3.12	−6.24		0.44	3.12	−3.92
Green 11:23 UT	1.85				4.17			
		0.55	3.60	−4.24		0.87	3.60	−6.71
Blue 14:59 UT	1.30				3.30			
13 May 2005	dimming 1				dimming 2			
White 17:37 UT	1.62				1.05			
		0.14	5.33	−0.73		0.13	5.33	0.67
Yellow 22:57 UT	1.48				1.18			
		0.03	10.65	−0.08		0.16	10.65	−0.42
Green 09:36 UT[a]	1.45				1.02			
		0.08	3.88	−0.57		0.30	3.88	−2.15
Blue 13:26 UT[a]	1.53				0.72			
06 July 2006	dimming 1				dimming 2			
White 20:31 UT	1.19				0.67			
		0.24	9.20	−0.72		0.29	9.20	−0.87
Yellow 05:43 UT[a]	0.95				0.38			
		0.98	3.40	−0.08		0.12	3.40	−0.11
Green 09:07 UT[a]	0.85				0.26			
		0.69	4.31	−0.44		0.15	4.31	−0.97
Blue 13:26 UT[a]	0.78				0.11			

[a]Denotes the event date plus one day.

2005 event (Figure 3) clearly shows dimming region 2, exhibiting a gradual increase in brightness as the time series progresses. Dimming region 1 is not so easily identified, but there is a sharp drop in intensity immediately to the West of the post-eruptive arcade (PEA) – the intensity level of this region remains approximately constant throughout the time series. We discuss possible reasons for this in the Appendix. The 6 July 2006 event (Figure 4) originates from an older, more dispersed active region than the other events – the intensity profile before the event (top left) reflects this, showing the more dispersed brightenings that correspond to the strong magnetic field concentrations of this active region. Both dimmings can be identified in the intensity profiles – especially the migratory nature of dimming 1 (discussed further in the Appendix), initially near to the PEA, moving East during the event. Dimming 1 settles to a relatively constant intensity level. Dimming 2 on the other hand, reaches its minimum intensity early on in the recovery phase, thereafter showing a progressive increase in intensity throughout the time series.

3.3. Light Curves Showing the Intensity Evolution and Structure of the Dimmings

At the top of Figures 5, 6 and 7 are base difference images near the maximum spatial extent of the dimmings. The green regions correspond to the full spatial extent of the dimmings as identified by the contour method. The orange core regions correspond to the longest-lived dimmings that still exist at the end of each dataset (see figure captions for details of times). Light curves of the average intensity within each region are plotted as a function of time. The onset of dimming in each event is clearly identifiable by a dramatic drop in intensity, followed by a gentle positive gradient, which we identify as the recovery phase of each event.

In each event (except dimming 1 of 13 May 2005 and 6 July 2006, see Appendix), the blue light curve (taken from the periphery of the dimmings) shows a full recovery to (or

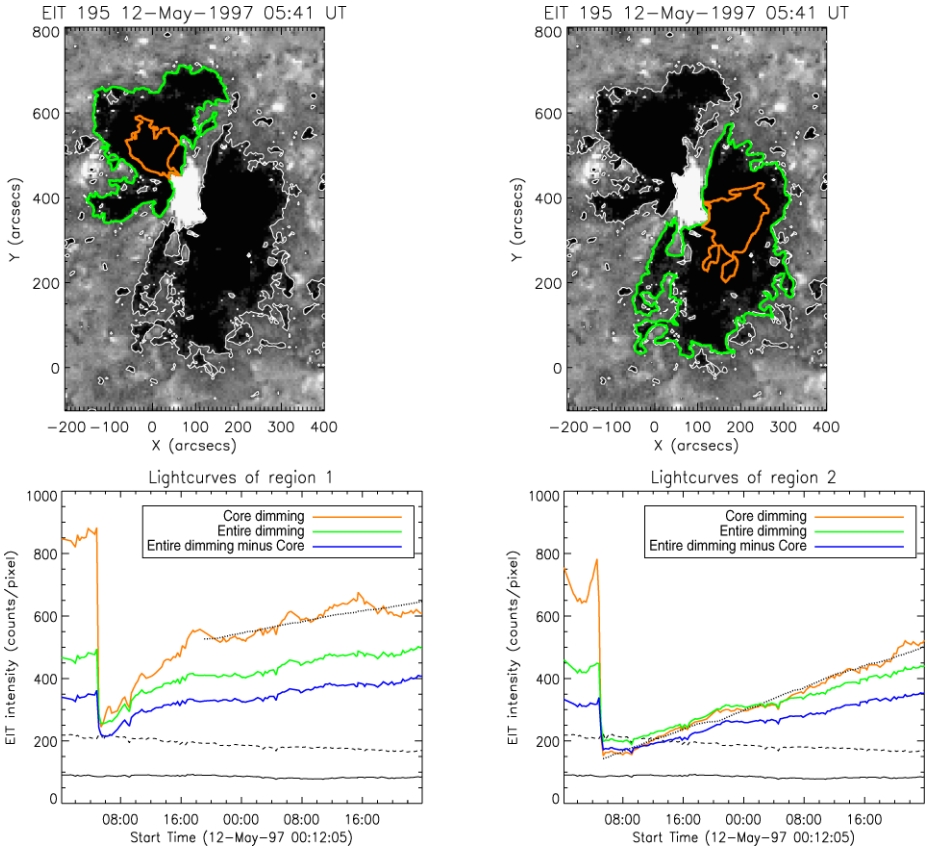

Figure 5 Top: Base-difference images showing 12 May 1997 dimmings with contours (white) overlaid at 05:41 UT. Green regions mark out the full extent of the dimming analysed in the bottom panels. Orange regions mark out the cores of these regions, corresponding to dimmings still existing at 23:55 UT on 13 May 1997. Light curves: Green light curves show the average intensity of the entire dimming region (marked in green in the images above). Orange light curves show the average intensity of just the core (orange) dimming region. Overlaid is the black dotted line of best fit calculated during the recovery phase. Blue light curves show the average intensity of the peripheral dimming region (the full dimming, minus the core of the dimming). The dashed line shows the intensity level in a region of quiet Sun, and the solid line indicates the intensity level in a pre-existing coronal hole for comparison.

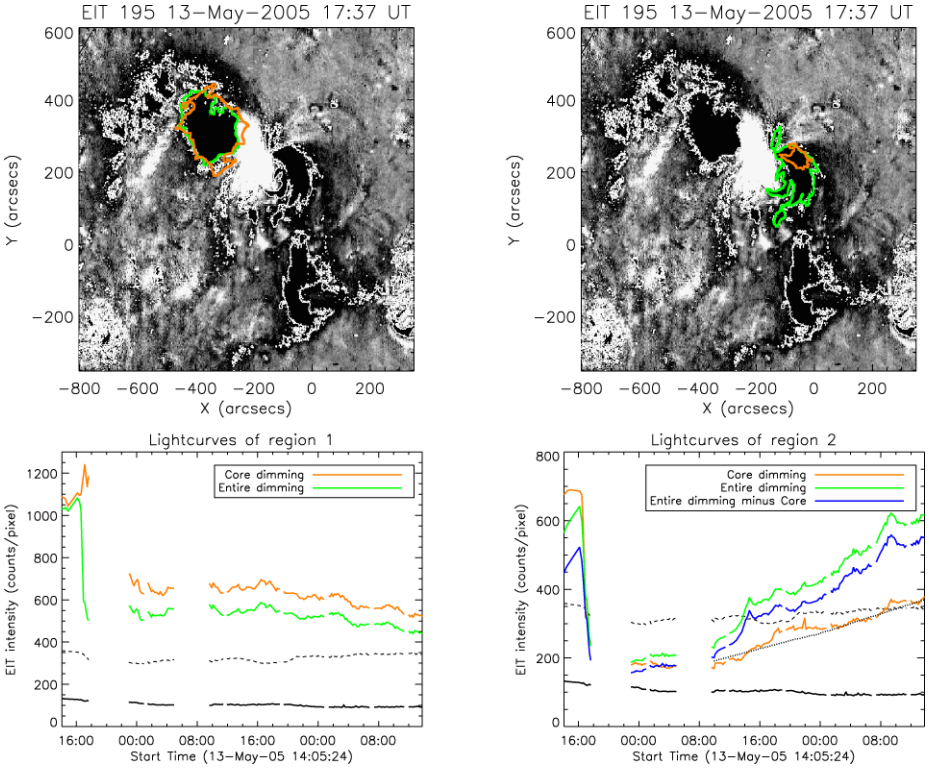

Figure 6 Top: Base-difference images showing 13 May 2005 dimmings with contours (white) overlaid at 17:37 UT. Green regions mark out the full extent of the dimming analysed in the bottom panels. Orange regions mark out the cores of these regions, corresponding to dimmings still existing at 13:47 UT on 15 May 2005. Light curves: Green light curves show the average intensity of the entire dimming region (marked in green in the images above). Orange light curves show the average intensity of just the core (orange) dimming region. Overlaid is the black dotted line of best fit calculated during the recovery phase. Blue light curves show the average intensity of the peripheral dimming region. Region 1 does not show a substantial difference between the full and core dimmings during our dataset, so the resulting peripheral light curve does not contribute substantially different data to that already displayed and is omitted. The dashed line shows the intensity level in a region of quiet Sun, and the solid line indicates the intensity level in a pre-existing coronal hole for comparison.

exceeding) pre-dimming intensity levels. In contrast, the orange light curves, showing the average intensity evolution of the cores of the dimmings, although generally exhibiting a constant, gradual recovery (exceptions: dimming 1 of 13 May 2005 and 6 July 2006, see Appendix) do not show a return to pre-event conditions by the end of these data sets. If we assume that the recovery gradient remains the same as that already displayed on the core light curve plots, then we can perform a least-square linear fit to the recovery part of the existing light curves and extrapolate the resulting fit to estimate the time at which the dimmings might reasonably be expected to recover to pre-event intensity levels. Table 2 shows the extrapolated recovery times for both the cores and the periphery of the dimmings for each event.

Even though they are located far from the outer boundaries of the dimmings, the cores of the dimmings start to show an increase in intensity very soon after the dimming has taken place. This is consistent with the results displayed by the intensity profiles in Figures 2, 3,

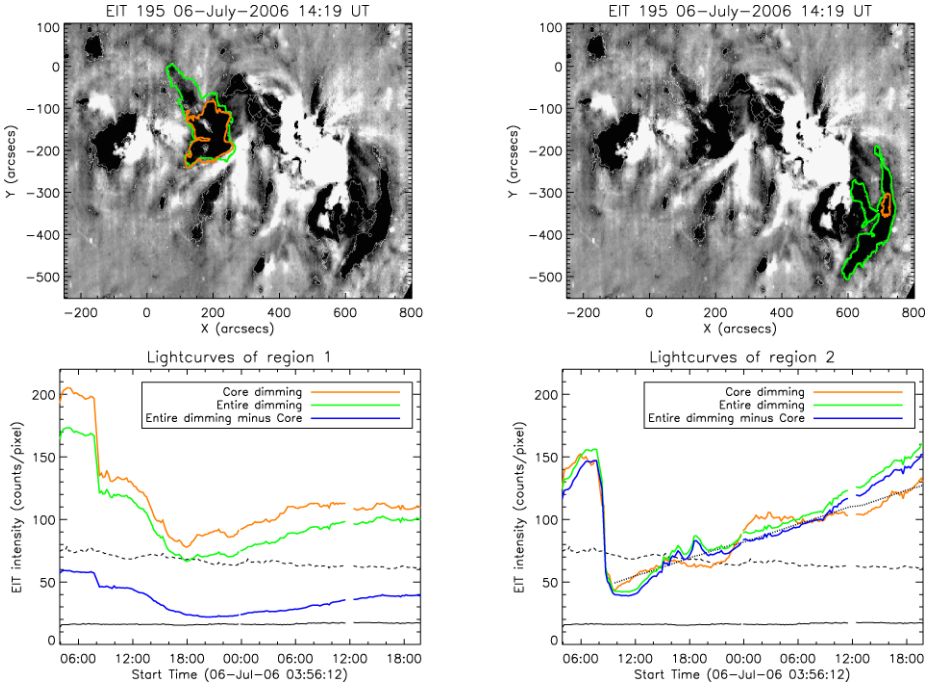

Figure 7 Top: Base-difference images showing 6 July 2006 dimmings with contours (white) overlaid at 20:31 UT. Green regions mark out the full extent of the dimming analysed in the bottom panels. Orange regions mark out the cores of these regions, corresponding to dimmings still existing at 19:48 UT on 7 July 2006. Light curves: Green light curves show the average intensity of the entire dimming region (marked in green in the images above). Orange light curves show the average intensity of just the core (orange) dimming region. Overlaid is the black dotted line of best fit calculated during the recovery phase. Blue light curves show the average intensity of the peripheral dimming region. The dashed line shows the intensity level in a region of quiet Sun, and the solid line indicates the intensity level in a pre-existing coronal hole for comparison.

Table 2 Extrapolated recovery times and lifetimes for the core and the periphery of the dimmings (assuming that the recovery gradient remains the same as that displayed in Figures 5, 6, and 7 – see Section 3.3). The start of the recovery time is defined by the minima of the light curves. The time difference between the recovery and the start times define the lifetime of the dimmings.

Event and dimming		Time core recovery (UT)	Time peripheral recovery (UT)	Lifetime core	Lifetime periphery
12 May 1997	1	16 May 1997 00:00	13 May 1997 04:00	92 h	22 h
	2	15 May 1997 02:00	13 May 1997 16:00	68 h	34 h
13 May 2005	1	No recovery	–	–	–
	2	17 May 2005 16:00	15 May 2005 07:00	89 h	32 h
06 July 2006	1	No recovery	–	–	–
	2	08 July 2006 06:00	07 July 2006 14:00	44 h	27 h

and 4, where the dimmings show an internal increase in intensity. Although the contour plots in Figures 2, 3, and 4 show that the dimmings do shrink from their outer boundaries inward, the intensity profiles in Figures 2, 3, 4 and the light curves of Figures 5, 6, 7 demonstrate that

there is also an internal contribution to the recovering intensity level. We refer the interested reader to the Appendix where we discuss additional features of the light curves.

To more directly understand the structure of the dimmings, we make 3D surface plots of the intensity within the dimmings when they are near their maximum spatial extent. Figure 8 shows 3D surface plots of the base difference data. The non-uniformity of the intensity within the dimmings is striking. A clear and consistent structure is evident in all events. The deepest dimming occurs adjacent to the bright PEA, with the extended dimming becoming gradually less intense with increasing distance from the PEA.

4. Physical Constraints Implied by the Observed Dimming Recovery

Our examination of the evolution of the dimming regions during the recovery phase has revealed several new results that must be taken into account when considering our understanding of the physical process(es) responsible for the recovery. We find that in all three studied cases, the dimmings shrink in their spatial extent, so recovering the intensity of the dimmed region from the outer boundary (see Figures 2, 3, and 4). We note that this shrinkage occurs in a fragmentary and inhomogeneous manner. This observation is consistent with the results of Kahler and Hudson (2001) who studied 19 dimmings with *Yohkoh*/SXT data (including the 12 May 1997 event studied here) and found that the dimmings tend to disappear "by a net contraction of the boundaries".

Interestingly, Kahler and Hudson (2001) specify that the net contraction of the boundaries is the only way in which the dimmings are observed to recover in *Yohkoh*/SXT data. They state that in none of the 19 cases they studied did they see the interior dimming brightness increase systematically with time. In contrast, in this work we have analysed EUV SOHO/EIT 195 Å data, and we have shown that there is a progressive increase of the intensity *within* the dimmings (see Figures 2, 3, 4, and 5, 6, 7). Such an internal recovery in intensity is not observed in *Yohkoh*/SXT data. We independently confirm this finding of Kahler and Hudson (2001) using *Yohkoh*/SXT data from the AlMg filter between 06:52 UT and 20:22 UT for the 12 May 1997 event (see Figure 9). The observation of internal brightening is observed in the SOHO/EIT 195 Å bandpass, which is dominated by Fe XII emission lines at 192.3, 193.5, and 195.1 Å corresponding to a characteristic formation temperature of $\approx 1.5 \times 10^6$ K at typical coronal densities. In contrast, *Yohkoh*/SXT detected plasma at temperatures $> 3 \times 10^6$ K. Thus *Yokhoh*/SXT and SOHO/EIT probe plasmas of different temperature. It would appear that during the recovery process there is not enough power to heat the plasma to a high enough temperature for detection in *Yohkoh*/SXT data.

The 3D surface plots showing the distribution of the intensity within the dimmings (Figure 8) are also in contrast with the data obtained by *Yohkoh*/SXT, with Kahler and Hudson (2001) noting the "uniformly dark interiors" of the dimmings they studied. The clear structure revealed here with SOHO/EIT data has implications for the study of coronal dimmings, particularly regarding the intensity change in these regions during the recovery phase. The structure of the dimming must be analysed carefully since the interpretation of the resulting variation in emission will heavily depend on the location selected for analysis; *e.g.* Table 2 shows how the "lifetime" of the dimming differs substantially between its core and periphery.

4.1. Recovery Does Not Necessarily Mean Disconnection

Our analysis shows that for the 12 May 1997 event, the average intensity of both the dimmings has recovered by the end of our dataset. Assuming the cores of the dimmings continue

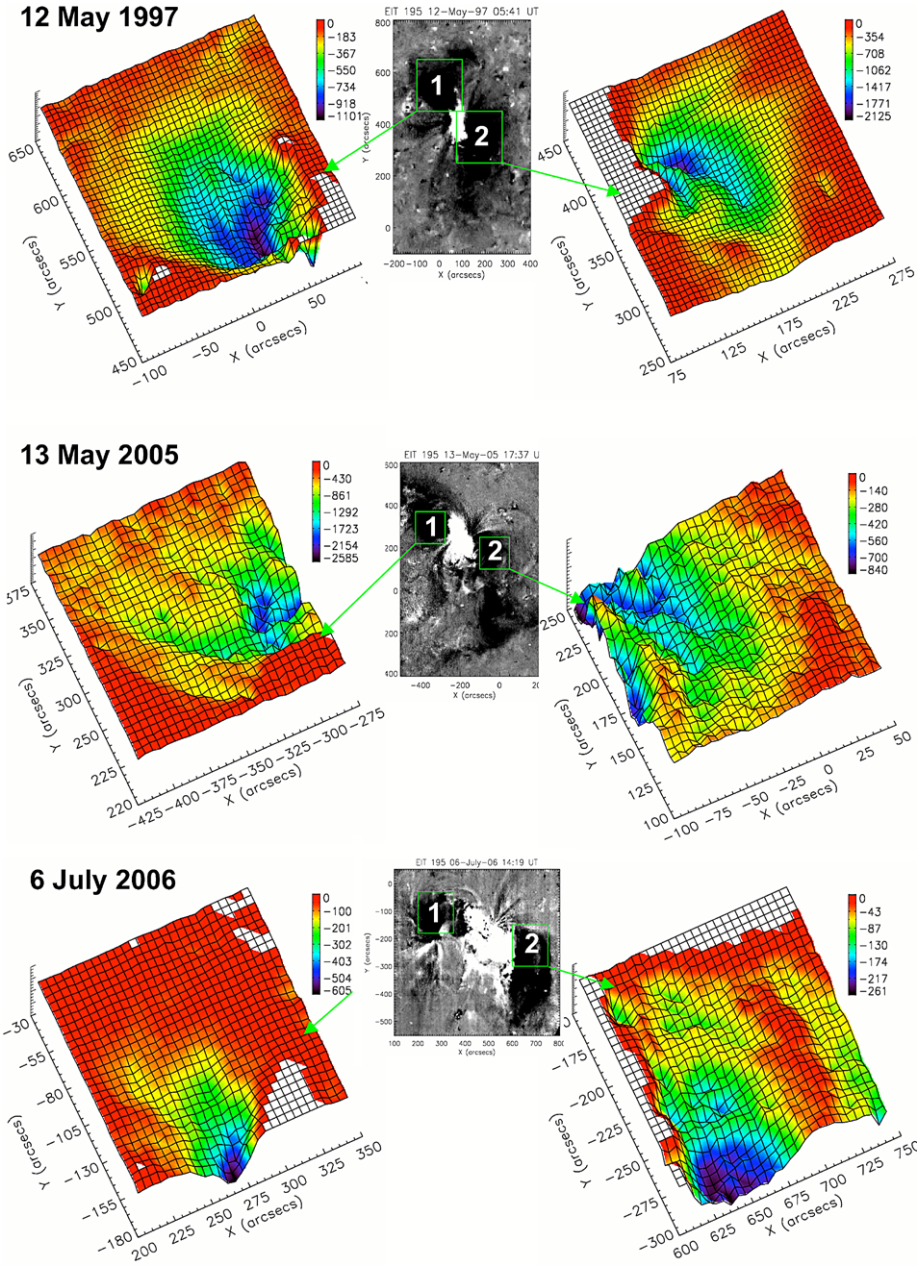

Figure 8 For each row, the central panel shows a base-difference image. Green boxes indicate data used to make 3D surface plots of intensity shown on the sides. The surface plots show the intensity change compared to the pre-event level (in counts pixel^{-1}). The regions of increased intensity are cut (where the surface is flat and white). The intensity of the dimmings is clearly non-uniform, with deeply dimmed regions located close to the post-eruptive arcade.

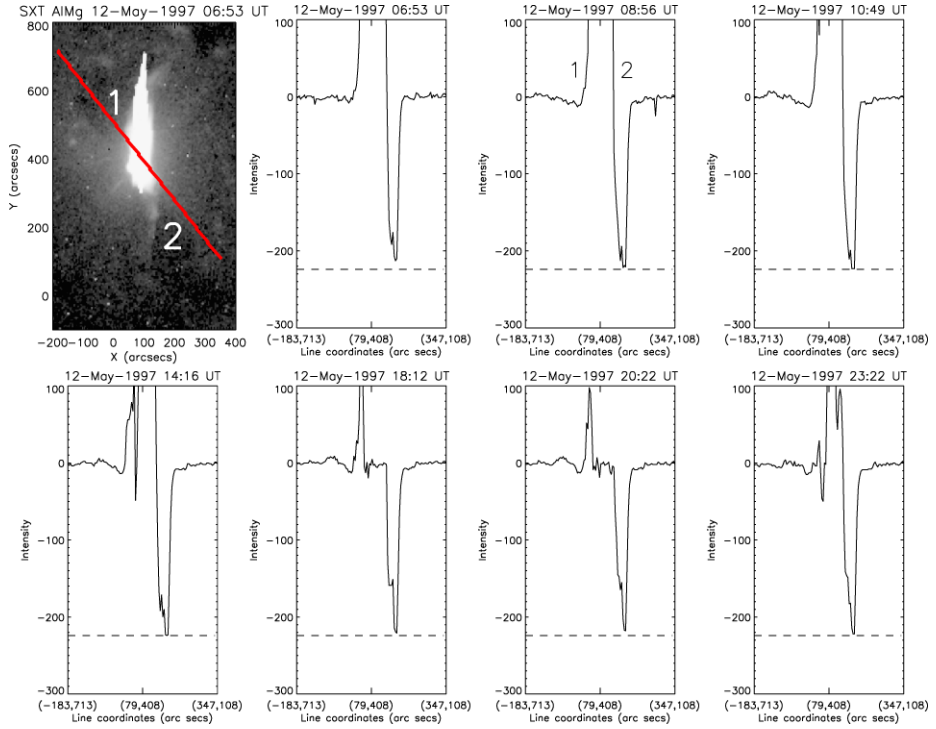

Figure 9 The top left panel is a *Yohkoh*/SXT AlMg filter intensity heliogram showing the 12 May 1997 dimmings. The red line overlaid shows the location of the data used to produce the following intensity profile plots. Intensity profile plots made along the red line (shown in the top left panel), at various times during the dimming recovery. The dimmings are identified by the numbers 1 and 2. The dashed line shows the deepest dimming level reached inside dimming 2 in this time series. The bright post-eruptive arcade coupled with the geometric projection effect largely obscures dimming region 1.

to recover at the rate displayed within our dataset, we have calculated that the core of dimming 1 is expected to recover by 00:00 UT on 16 May, and the core of dimming 2 by 02:00 UT 15 May (see Section 3.3 and Table 2). However, from 10:00 UT to ≈ 22:00 UT on 15 May, unidirectional electrons from a positive source are detected at 1 AU (see Section 2.1). The travel time to 1 AU for the slowest electrons is six hours (Larson *et al.*, 1997). Taking this electron travel time into account, unidirectional electrons must leave the Sun between 04:00 UT and ≈ 16:00 UT 15 May. Dimming 2 is the positive-polarity dimming (Attrill *et al.*, 2006), so we observe a unidirectional electron stream from the positive-polarity dimming even though that core dimming is expected to have recovered in intensity and disappeared by 02:00 UT on 15 May.

For the 13 May 2005 event, Qiu *et al.* (2007) identify the MC duration from 05:40 UT on 15 May to 04:40 UT on 16 May (see Section 2). During this interval the cores of both dimmings remain unrecovered, so the presence of bidirectional electron heat fluxes is expected.

For the 6 July 2006 event, the average intensity of the core of dimming 2 is expected to have recovered by 06:00 UT on 8 July. The light curves for dimming 1 (Figure 7) tend toward a zero gradient, so we cannot infer any information about the recovery rate from this data. The candidate for the interplanetary MC counterpart of this eruption in Figure 1(c) shows a unidirectional electron stream originating from a negative solar source, after

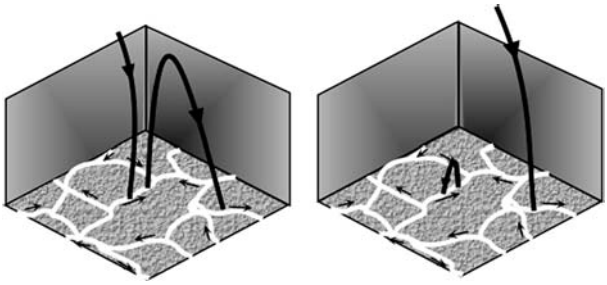

Figure 10 Figure 1 from Fisk and Zurbuchen (2006) illustrating the interaction between "open" magnetic field lines and small coronal loops. Left shows the pre-reconnection configuration comprising an "open" magnetic field line and a closed magnetic loop. Right shows the post-reconnection configuration and the displacement of the "open" magnetic field line.

$\approx$ 21:30 UT on 10 July. So we observe a unidirectional electron stream, presumably from the negative polarity dimming (region 2), even though dimming 2 is estimated to have recovered in intensity by 06:00 UT on 8 July.

Either, as Kahler and Hudson (2001) query, dimmings are not the source regions of the subsequent magnetic cloud (and associated electron heat fluxes), or, if they are the source regions (as considered by Webb *et al.* (2000); Mandrini *et al.* (2005); Attrill *et al.* (2006)), then we need to reconcile how the dimmings recover, yet the magnetic connection of the ICME/MC to the Sun is maintained.

4.2. Constraints that our Analysis Places on Possible Theories

In view of our results and the discussion above, we consider that any potential recovery mechanism must be capable of explaining shrinkage of the dimmings, internal brightenings, the relatively low temperature/low power produced in the dimmings during the recovery, all whilst still maintaining the magnetic connectivity of the ejecta to the Sun. For the intensity in the dimmings to recover, plasma must be present to generate the emission. Thus we expect that to constrain the plasma, the magnetic field must form closed flux tubes. In particular then, we consider the question of what is the physical process by which dimmings recover in intensity and how do they change from being regions of "open" to re-establish closed magnetic field?

McIntosh *et al.* (2007) discuss the post-eruptive evolution of the dimmings on 6 July 2006. They report the reintroduction of moss spreading outward from the active region and interpret this as the post-CME closure of the global coronal field above the active region following "disconnection" of the CME. In cases where the core dimmings are located adjacent to the PEA, the core dimmings are expected to shrink as the PEA expands, thus the recovery can indeed be at least partially due to closing-down of "opened" field lines, in accordance with the results of McIntosh *et al.* (2007). However, dimmings extend considerably far out into the quiet-Sun magnetic field (Webb *et al.*, 2000; Mandrini *et al.*, 2005; Attrill *et al.*, 2006), away from the active region and the domain where moss is observed (Berger *et al.*, 1999).

Rather than purely a *closure* of the global coronal magnetic field, we consider that interchange reconnections between the "open" magnetic field of the dimming, small coronal loops and emerging flux bipoles may act to *disperse* the concentration of "open" magnetic field forming the dimming out into the surrounding quiet Sun. Reconnections with closed

loops will "step" the "open" magnetic field out of the dimming (dispersing the "open" flux), whilst reconnection with "open" magnetic field will physically disconnect the magnetic field line from the Sun. Given the detection of electron heat fluxes at 1 AU after the dimmings are expected to recover, we consider that the most dominant process should be reconnection with closed magnetic field, which acts to disperse the "open" magnetic field out into regions of quiet Sun, thus recovering the intensity of the dimming whilst maintaining the magnetic connectivity to the Sun.

In the following, we analyse the processes which are expected to participate in the recovery of the dimmings. Reconnections should occur dominantly at the outer boundaries of dimmings (as suggested by Kahler and Hudson, 2001), where the "open" magnetic flux can interact most with surrounding quiet Sun magnetic field. The interchange reconnections at the outermost boundary of dimmings should occur in a similar manner to the flux emergence/expansion near coronal holes as shown by Baker, van Driel-Gesztelyi, and Attrill (2007). They find that interchange reconnections produce bright closed loops between the "open" field of the coronal hole and the bipolar region, whilst "stepping" the "open" field out of the coronal hole region. In our case, the bright loops at the boundary of the dimming would act to shrink the outer boundary at the point of interaction (as observed), whilst at the same time dispersing the "open" magnetic field of the dimming.

Within the dimming, there is also the possibility of reconnection between the "open" field and the existing field as well as emerging bipoles. Fisk and Zurbuchen (2006) note that within coronal holes (in our case dimmings), small loops are indeed observed to be present. These loops are interpreted as the result of localised reconnection (they are equivalent, at smaller scales, to flare loops). This idea finds support in the work of Larson *et al.* (1997) who interpreted the localised patches of brightening within a dimming as energy release at the footpoint of an interplanetary magnetic cloud, resulting from 3D field line reconnection.

Emerging flux, most probably in the form of ephemeral regions, also contributes to the recovery process within the dimming. In quiet-Sun regions, the timescale for flux replenishment by emergence was found to be between 1.5 and 3 days (Schrijver *et al.*, 1997). On comparison with the lifetimes of the dimmings shown in Table 2, it is apparent that such a timescale is sufficient for the recovery of the peripheral regions of the dimmings, but in some cases the cores remain dimmed for longer.

4.3. Implications of Reconnections Within the Dimmings

The emergence of new ephemeral regions brings closed loops into the "open" magnetic field environment of the dimmings, likely driving interchange reconnections which would have the effect of "opening" the emerged loops and evacuating the plasma they contain. (This would actually sustain dimming so effectively decreasing the rate of recovery of the dimmings, compared to the case with emergence but without reconnection.) Within the dimmings, the "open" flux remains, it is not so subjected to the "stepping out" by interchange reconnections with surrounding quiet-Sun loops. So the internal recovery is expected to be a slower process than the one at the periphery. A test of this would be to see how long outflows are measured in the cores of the dimmings. If outflows are measured at the beginning, as expected during the initial creation of the dimmings and then they stop, it would indicate recovery just by emergence of new closed loops without any interaction with pre-existing magnetic field. But if outflows are maintained well into the recovery phase, then it shows that interchange reconnections are continually occurring between the previously "opened" field and the newly emerged flux, allowing plasma to escape out into the solar wind. *Hinode*/EIS would be the ideal instrument with which to test this expected observational signature.

The above is also plausibly a key process responsible for forming the fast solar wind in coronal holes. Just as in dimmings, the new emerging flux in coronal holes is able to provide both the plasma and the magnetic energy to accelerate it, whilst the reconnected "open" field permits the escape of the plasma. However in coronal holes the emergence rate is significantly smaller (Zhang, Ma, and Wang, 2006; Abramenko, Fisk, and Yurchyshyn, 2006), than for the quiet Sun (Schrijver *et al.*, 1997), so the mean expected Doppler signal is expected to be much weaker in coronal holes than in dimmings. For a consistent, but different, result see Hagenaar, DeRosa, and Schrijver (2008).

The interchange reconnections between emerging flux and "open" field are expected to occur in very episodic (as opposed to continuous) events. Such a mechanism provides a natural origin of the very patchy nature of electron heat fluxes observed frequently in MCs and ICMEs.

4.4. Mechanisms for Dispersal of "Open" Magnetic Field

The main area of the dimming extends out into, and is surrounded by, regions of quiet-Sun magnetic field. The quiet-Sun magnetic field is subject to transport by convective motions, leading to its "diffusion" (*e.g.*, Hagenaar *et al.*, 1999).

If the location of a magnetic-field-line footpoint is displaced a distance r in a time t, then the "diffusion coefficient" (rate of dispersal of flux) is given by:

$$D \equiv \frac{\langle r^2 \rangle}{4t}. \tag{1}$$

Hagenaar *et al.* (1999) find that the diffusion coefficient of small-scale flux by granular buffeting is dominated by large-scale drifts which on timescales > 24 hours, randomises into a second diffusive motion where both small- and large-scale dispersal processes combine to give a "diffusion coefficient" of 284 km^2 s^{-1}. Comparison of the Hagenaar *et al.* (1999) "diffusion coefficient" with the rate of change in area of the dimmings for the three events of this study (see Table 1) shows that the dispersal of the "open" magnetic field of the dimmings due to granular buffeting alone is inadequate to explain the observed recovery rates of the dimmings.

Fisk and Schwadron (2001), Fisk (2005), and Fisk and Zurbuchen (2006) developed a model of interchange reconnection between "open" and closed magnetic field. They primarily discuss their model in a global context, but we suggest that it also appears to apply to the recovery phase of dimmings. In this approach, reconnection between the "open" magnetic field of the dimmings and the surrounding quiet-Sun magnetic field would act to accelerate the convective dispersal process described above by extending the distance (r) by which a magnetic-field-line footpoint is displaced (see Figure 10). Fisk and Schwadron (2001) consider that if there are numerous, randomly-orientated loops in the low corona, then the reconnection mechanism illustrated by Figure 10 can be described as a diffusive process. The interaction between "open" flux and closed loops is captured by the "diffusion coefficient" (κ):

$$\kappa = \frac{(\delta h)^2}{2\delta t}, \tag{2}$$

where δh is the displacement (related to the loop size) and where δt is the characteristic time for reconnection with the loops.

Fisk and Schwadron (2001) estimate κ in the quiet Sun, outside a coronal hole at low latitudes. They use $\delta h \approx 2 \times 10^{10}$ cm, an average value for the loop height, since although

the displacement distance should be on the order of twice the loop height, reconnection may occur anywhere along the loop. They use $\delta t \approx 1.5 \times 10^5$ seconds (38 hours), derived from the characteristic time for reconnection with loops at low latitudes. Using these values, the diffusion coefficient is calculated to be $\kappa \approx 1.6 \times 10^5$ km^2 s^{-1}. A comparison of this estimated rate of dispersal of "open" flux with the measured rate of recovery of the dimmings examined in this study (Table 1) shows a very good agreement. This validates our application of the Fisk and Schwadron (2001) model as a likely mechanism via which the recovery in intensity of dimmings is primarily achieved.

Since the recovery process is essentially a relaxation process (lacking the strong coherent driver of the CME expansion), the interchange reconnections would not be expected to form strong current sheets (as, *e.g.*, in a flare). We conclude that the lack of power generated by the interchange reconnection recovery process is therefore expected and supports the identification of many small-scale interchange reconnections with low-coronal quiet-Sun loops as the primary candidate for the mechanism facilitating recovery of the dimmings. We expect that the speed of recovery is closely related to the magnetic environment in which the dimmings form, proceeding faster in a quiet-Sun environment, while a much slower recovery is expected for dimmings formed in a strong monopolar magnetic environment, where there is little opposite-polarity flux present. This expectation will be tested and the results presented in a follow-up paper.

5. Conclusions

We consider why and how CME-related dimmings (identified as the footpoints of magnetic flux ropes in the interplanetary space), recover, despite the "open" magnetic connectivity to the Sun being maintained as indicated by electron heat flux measurements at 1 AU. Study of the intensity evolution of dimmings using SOHO/EIT data shows that they recover by shrinking of their outer boundaries as well as by internal brightenings that we consider are constrained to the low corona. We show that the SOHO/EIT dimmings have a clear spatial structure, with a deeply dimmed core gradually progressing to a lesser-dimmed periphery.

We propose that *i*) the recovery of the dimmings by shrinking from their outer edges occurs mainly by interchange reconnection with existing closed quiet-Sun loops and emerging bipoles and *ii*) that the internal recovery of the dimmings can be due to emergence of new closed loops (ephemeral regions) that bring new plasma into the dimmings.

We quantitatively demonstrate that the model developed in Fisk and Schwadron (2001) of interchange reconnections between "open" magnetic field and small coronal loops is a strong candidate for the primary mechanism facilitating the recovery of the dimmings. The interchange reconnections disperse the concentration of "open" magnetic field forming the dimming out into the surrounding quiet Sun. This process acts to generate the apparent recovery in intensity of the dimming, whilst still maintaining the magnetic connectivity to the Sun.

Acknowledgements We sincerely thank the anonymous referee for helpful comments, which improved the clarity and readability of this work. G.D.R.A and K.S. are grateful to STFC for support. L.v.D.G. acknowledges Hungarian government grant OTKA T048961. P.D. and C.H.M. acknowledge financial support from CNRS (France) and CONICET (Argentina) through their cooperative science programme (N. 20326). A.N.Z. acknowledges support from the Belgian Federal Science Policy Office through the ESA-PRODEX programme. J.L. was supported by NASA and CISM, an NSF Science and Technology Center.

Appendix

We offer further discussion regarding the light curves shown in Figures 5, 6, and 7.

Although the minimum average intensity for both the core (orange) and the entire dimming (green) regions (periphery + core) reach similar intensity levels (Figures 5, 6, and 7), for the May 1997 event, the average intensity of the core region tends to exceed that of the periphery throughout the datasets – both before and during the manifestation of the dimmings. The original EIT data (not the base-difference images), shows that a sigmoid structure reforms on 13 May 1997 (especially visible at 14:50 UT). So together with the sigmoid on 12 May before the eruption, the intensity of the core region is high before the event, dims during the eruption, and then recovers to a level significantly higher than the periphery again, due to the reformation of the sigmoid in the vicinity of the core regions.

We note that the light curve of dimming 1 (13 May 2005) does not show any tendency toward recovery during our dataset (Figure 6). Before the eruption, the source region is highly sheared, showing a sigmoidal structure. The sigmoid has oppositely curved "elbows" at each end, where the elbows appear to be illuminated strands of the sigmoidal core field (see Moore *et al.*, 2001). The eruption of the core field blows away these elbow loop structures, exposing the quiet Sun underneath. Due to the large PEA that forms following the eruption, and the considerable projection of the PEA onto the location of dimming 1, we consider that possibly we do not actually observe the core dimming of the north end of the flux rope in this event. It may well be obscured by the PEA. This interpretation is supported by the light curves in Figure 6 which remain significantly above the intensity of an undisturbed area of quiet Sun during the whole event, consistent with the exposure of background quiet Sun after the overlying sigmoidal structure relaxed following the eruption. We note that the disappearance of a large-scale coronal feature seen by *Yohkoh*/SXT, similarly leading to a coronal dimming was documented by Hudson, Acton, and Freeland (1996).

Dimming 1 of 6 July 2006 also shows a comparatively unusual evolution – instead of a straightforward dramatic drop in intensity at the onset of the dimming as in the other light curves, the progression toward minimum intensity is more gradual, taking place over $\approx$ ten hours. The recovery of the light curves for the 6 July 2006 event levels to an approximately zero gradient near the end of our dataset. In the SOHO/EIT 284 Å heliogram at 07:01 UT (not shown) there are large-scale loops extending from the positive dimming 1 to a remote negative polarity located Northwest of AR 10898. During the course of the eruption, it is clear that these large-scale loops are successively "opened" up (visible in the SOHO/EIT 284 Å movie from 07:01 UT – 19:01 UT), which we suggest may lead to the somewhat migratory movement of dimming region 1. Initially dimming region 1 is close to the PEA at 09:19 UT, apparently at the same location as the footpoint of an erupting filament (visible in emission in the SOHO/EIT 195 Å movie), then the dimming progressively migrates to the Northwest, reaching its furthest extent from the PEA by about 16:30 UT. The disruption of large-scale loops leading to coronal dimming at their footpoints is a well-documented feature of solar eruptions (Manoharan *et al.*, 1996; Khan and Hudson, 2000; Delannée, 2000; Harra *et al.*, 2007a) and may facilitate the continued "openness" and prolonged lifetime of dimming 1 in this event.

References

Abramenko, V.I., Fisk, L.A., Yurchyshyn, V.B.: 2006, *Astrophys. J.* **641**, L65.

Attrill, G., Nakwacki, M.S., Harra, L.K., van Driel-Gesztelyi, L., Mandrini, C.H., Dasso, S., Wang, J.: 2006, *Solar Phys.* **238**, 117.

Attrill, G.D.R., Harra, L.K., van Driel-Gesztelyi, L., Démoulin, P., Wülser, J.P.: 2007, *Astron. Nachr.* **328**, 760.
Baker, D., van Driel-Gesztelyi, L., Attrill, G.D.R.: 2007, *Astron. Nachr.* **328**, 773.
Berger, T.E., de Pontieu, B., Fletcher, L., Schrijver, C.J., Tarbell, T.D., Title, A.M.: 1999, *Solar Phys.* **190**, 409.
Burlaga, L., Sittler, E., Mariani, F., Schwenn, R.: 1981, *J. Geophys. Res.* **86**, 6673.
Chertok, I.M., Grechnev, V.V.: 2003, *Astron. Nachr.* **47**, 934.
Chertok, I.M., Grechnev, V.V.: 2005, *Solar Phys.* **229**, 95.
Chertok, I.M., Grechnev, V.V., Hudson, H.S., Nitta, N.V.: 2004, *J. Geophys. Res.* **109**(A18), 2112.
Crooker, N.U., Webb, D.F.: 2006, *J. Geophys. Res.* **111**(A10), 8108.
Crooker, N.U., Gosling, J.T., Kahler, S.W.: 2002, *J. Geophys. Res.* **107**, 1028.
Culhane, J.L., Harra, L.K., James, A.M., Al-Janabi, K., Bradley, L.J., Chaudry, R.A., Rees, K., Tandy, J.A., Thomas, P., Whillock, M.C.R., *et al.*: 2007, *Solar Phys.* **243**, 19.
de Toma, G., Holzer, T.E., Burkepile, J.T., Gilbert, H.R.: 2005, *Astrophys. J.* **621**, 1109.
Delaboudinière, J.P., Artzner, G.E., Brunaud, J., Gabriel, A.H., Hochedez, J.F., Millier, F., Song, X.Y., Au, B., Dere, K.P., Howard, R.A., *et al.*: 1995, *Solar Phys.* **162**, 291.
Delannée, C.: 2000, *Astrophys. J.* **545**, 512.
Démoulin, P.: 2008, *Ann. Geophys.*, in press.
Fisk, L.A.: 2005, *Astrophys. J.* **626**, 563.
Fisk, L.A., Schwadron, N.A.: 2001, *Astrophys. J.* **560**, 425.
Fisk, L.A., Zurbuchen, T.H.: 2006, *J. Geophys. Res.* **111**(A10), 9115.
Hagenaar, H.J., DeRosa, M.L., Schrijver, C.J.: 2008, *Astrophys. J.* **678**, 541.
Hagenaar, H.J., Schrijver, C.J., Title, A.M., Shine, R.A.: 1999, *Astrophys. J.* **511**, 932.
Hansen, R.T., Garcia, C.J., Hansen, S.F., Yasukawa, E.: 1974, *Pub. Astron. Soc. Pac.* **86**, 500.
Harra, L.K., Sterling, A.C.: 2001, *Astrophys. J.* **561**, L215.
Harra, L.K., Crooker, N.U., Mandrini, C.H., van Driel-Gesztelyi, L., Dasso, S., Wang, J., Elliott, H., Attrill, G., Jackson, B.V., Bisi, M.M.: 2007a, *Solar Phys.* **244**, 95.
Harra, L.K., Hara, H., Imada, S., Young, P., Williams, D.R., Sterling, A.C., Korendyke, C., Attrill, G.D.R.: 2007b, *Pub. Astron. Soc. Japan* **59**, S801.
Harrison, R.A., Sawyer, E.C., Carter, M.K., Cruise, A.M., Cutler, R.M., Fludra, A., Hayes, R.W., Kent, B.J., Lang, J., Parker, D.J., *et al.*: 1995, *Solar Phys.* **162**, 233.
Hudson, H.S., Cliver, E.W.: 2001, *J. Geophys. Res.* **106**, 25199.
Hudson, H.S., Acton, L.W., Freeland, S.L.: 1996, *Astrophys. J.* **470**, 629.
Imada, S., Hara, H., Watanabe, T., Asai, A., Kamio, S., Matsuzaki, K., Harra, L.K., Mariska, J.T.: 2007, *Pub. Astron. Soc. Japan* **59**, S793.
Jiang, Y., Yang, L., Li, K., Ren, D.: 2007, *Astrophys. J.* **662**, L131.
Kahler, S.W., Hudson, H.S.: 2001, *J. Geophys. Res.* **106**, 29239.
Khan, J.I., Hudson, H.S.: 2000, *Geophys. Res. Lett.* **27**, 1083.
Larson, D.E., Lin, R.P., McTiernan, J.M., McFadden, J.P., Ergun, R.E., McCarthy, M., Rème, H., Sanderson, T.R., Kaiser, M., Lepping, R.P., *et al.*: 1997, *Geophys. Res. Lett.* **24**, 1911.
Lepping, R.P., Acũna, M.H., Burlaga, L.F., Farrell, W.M., Slavin, J.A., Schatten, K.H., Mariani, F., Ness, N.F., Neubauer, F.M., Whang, Y.C., *et al.*: 1995, *Space Sci. Rev.* **71**, 207.
Lin, R.P., Anderson, K.A., Ashford, S., Carlson, C., Curtis, D., Ergun, R., Larson, D., McFadden, J., McCarthy, M., Parks, G.K., *et al.*: 1995, *Space Sci. Rev.* **71**, 125.
Liu, C., Lee, J., Yurchyshyn, V., Deng, N., Cho, K.S., Karlický, M., Wang, H.: 2007, *Astrophys. J.* **669**, 1372.
Malandraki, O.E., Lario, D., Lanzerotti, L.J., Sarris, E.T., Geranios, A., Tsiropoula, G.: 2005, *J. Geophys. Res.* **110**(A9), 09S06.
Mandrini, C.H., Pohjolainen, S., Dasso, S., Green, L.M., Démoulin, P., van Driel-Gesztelyi, L., Copperwheat, C., Foley, C.: 2005, *Astron. Astrophys.* **434**, 725.
Mandrini, C.H., Nakwacki, M.S., Attrill, G., van Driel-Gesztelyi, L., Démoulin, P., Dasso, S., Elliott, H.: 2007, *Solar Phys.* **244**, 25.
Manoharan, P.K., van Driel-Gesztelyi, L., Pick, M., Demoulin, P.: 1996, *Astrophys. J.* **468**, L73.
McComas, D.J., Gosling, J.T., Phillips, J.L., Bame, S.J., Luhmann, J.G., Smith, E.J.: 1989, *J. Geophys. Res.* **94**, 6907.
McIntosh, S.W., Leamon, R.J., Davey, A.R., Wills-Davey, M.J.: 2007, *Astrophys. J.* **660**, 1653.
Moore, R.L., Sterling, A.C., Hudson, H.S., Lemen, J.R.: 2001, *Astrophys. J.* **552**, 833.
Owens, M.J., Crooker, N.U.: 2007, *J. Geophys. Res.* **112**, 6106.
Qiu, J., Hu, Q., Howard, T.A., Yurchyshyn, V.B.: 2007, *Astrophys. J.* **659**, 758. doi:10.1086/512060.
Richardson, I.G., Farrugia, C.J., Burlaga, L.F.: 1991, In: Cawley, M., *et al.* (eds.) *22nd International Cosmic Ray Conference* **3**, 597.
Riley, P., Gosling, J.T., Crooker, N.U.: 2004, *Astrophys. J.* **608**, 1100.

Rust, D.M.: 1983, *Space Sci. Rev.* **34**, 21.
Rust, D.M., Hildner, E.: 1976, *Solar Phys.* **48**, 381.
Schrijver, C.J., Title, A.M., van Ballegooijen, A.A., Hagenaar, H.J., Shine, R.A.: 1997, *Astrophys. J.* **487**, 424.
Shodhan, S., Crooker, N.U., Kahler, S.W., Fitzenreiter, R.J., Larson, D.E., Lepping, R.P., Siscoe, G.L., Gosling, J.T.: 2000, *J. Geophys. Res.* **105**, 27261.
Smith, C.W., L'Heureux, J., Ness, N.F., Acuña, M.H., Burlaga, L.F., Scheifele, J.: 1998, *Space Sci. Rev.* **86**, 613.
Sterling, A.C., Hudson, H.S.: 1997, *Astrophys. J.* **491**, L55.
Thompson, B.J., Plunkett, S.P., Gurman, J.B., Newmark, J.S., St. Cyr, O.C., Michels, D.J.: 1998, *Geophys. Res. Lett.* **25**, 2465.
Thompson, B.J., Cliver, E.W., Nitta, N., Delannée, C., Delaboudinière, J.P.: 2000, *Geophys. Res. Lett.* **27**, 1431.
Tsuneta, S., Acton, L., Bruner, M., Lemen, J., Brown, W., Caravalho, R., Catura, R., Freeland, S., Jurcevich, B., Owens, J.: 1991, *Solar Phys.* **136**, 37.
Vaiana, G.S., van Speybroeck, L., Zombeck, M.V., Krieger, A.S., Silk, J.K., Timothy, A.: 1977, *Space Sci. Instr.* **3**, 19.
Webb, D.F., Lepping, R.P., Burlaga, L.F., DeForest, C.E., Larson, D.E., Martin, S.F., Plunkett, S.P., Rust, D.M.: 2000, *J. Geophys. Res.* **105**, 27251.
Yurchyshyn, V., Liu, C., Abramenko, V., Krall, J.: 2006, *Solar Phys.* **239**, 317.
Zarro, D.M., Sterling, A.C., Thompson, B.J., Hudson, H.S., Nitta, N.: 1999, *Astrophys. J.* **520**, L139.
Zhang, J., Ma, J., Wang, H.: 2006, *Astrophys. J.* **649**, 464.
Zhukov, A.N., Auchère, F.: 2004, *Astron. Astrophys.* **427**, 705.